International Journal of Solids and Structures 51 (2014) 1299–1310

Contents lists available at ScienceDirect

International Journal of Solids and Structures

journal homepage: www.elsevier.com/locate/ijsolstr

A continuum based modelling approach for adhesively bonded piezo-transducers for EMI technique

Sumedha Moharana, Suresh Bhalla *

Department of Civil Engineering, Indian Institute of Technology Delhi, Hauz Khas, New Delhi 110016, India

ARTICLE INFO

Article history:
Received 28 January 2013
Received in revised form 9 December 2013
Available online 19 December 2013

Keywords:
Piezo-impedance transducer
Electro-mechanical impedance (EMI) technique
Shear lag
Admittance signature
Refined model and continuum based model

ABSTRACT

In the electro-mechanical impedance (EMI) technique, which is based on induced strain actuation through piezoelectric ceramic (PZT) patch, the knowledge of shear stress distribution in the adhesive bond layer between the patch and the host structure is very pertinent for reliable health monitoring of structures. The analytical derivation of continuum based shear lag model covered in this paper aims to provide an improved and more accurate model for shear force interaction between the host structure and the PZT patch (assumed square for simplicity) through the adhesive bond layer, taking care of all the piezo, structural and adhesive effects rigorously and simultaneously. Further, it eliminates the hassle of determining the equivalent impedance of the structure and the actuator separately, as required in the previous models, which was approximate in nature. The results are compared with the previous models to highlight the higher accuracy of the new approach. Based on the new model, a continuum based interaction term has been derived for quantification of the shear lag and inertia effects.

1. Introduction

The impedance based structural health monitoring (SHM) techniques have utilized the electro-mechanical coupling property of piezoelectric materials (piezo-impedance transducers), due to their self-sensing nature (ability to act both as actuators and sensors), and has the potential to minimize the maintenance and inspection cost of engineering structures. For the past few years, the piezoelectric ceramic (PZT) patches have demonstrated their suitability for SHM as part of the electro-mechanical impedance (EMI) technique for a wide variety of structures (Sun et al., 1995; Soh et al., 2000; Park et al., 2000a, 2000b; Lim et al., 2006; Giurgiutiu and Zagrai, 2000, 2002; Bhalla and Soh, 2003, 2004a, 2004b, 2004c; Bhalla et al., 2005; Shanker et al., 2011). The basic principle of the EMI technique for SHM is to monitor the integrity of the structure by measuring the electrical admittance of the PZT transducer bonded on surface of the monitored structure. Because of the direct and the converse piezoelectric effects, any change in the mechanical impedance of the structure caused by damage modifies the electrical admittance of the PZT transducer bonded to it. Usually, the electro-mechanical admittance signature, comprising of the conductance (real part) and the susceptance (imaginary part) is acquired from the bonded patch in the healthy condition of the structure and used as the reference baseline for future decisions on the structural integrity. Any damage on the structure modifies the admittance signature, thereby providing a signal to the user.

The electromechanical constitutive equations for linear material behaviour can be expressed as (IEEE standards, 1987)

$$D_3 = \overline{\varepsilon_{33}^T} E_3 + d_{31} T_1 \tag{1}$$

$$S_1 = \frac{T_1}{\overline{Y^E}} + d_{31} E_3 \tag{2}$$

where (referring to Fig. 1) T_1 and S_1 are stress and strain respectively along axis (1), d_{31} the piezoelectric strain coefficient, D_3 the charge density, E_3 the electric field along axis (3) and $\overline{\varepsilon_{33}^T}$ and $\overline{Y^E}$ the complex electric permittivity and Young's modulus of the patch respectively.

Several researchers have attempted to capture the PZT-structure interaction mechanism through their models which are briefly reviewed here. Crawley and de Luis (1987) proposed the static approach, which idealized the structure as a spring, connected to the PZT patch and excited by alternating electrical field (E_3), as illustrated in Fig. 1(a). They derived the equilibrium strain (S_{eq}) from quasi static equilibrium of the system as

$$S_{eq} = \frac{d_{31} E_3}{1 + \left(\frac{k_s l}{\overline{Y^E} w_p h_p}\right)} \tag{3}$$

where l, w_p and h_p are the half- length, the width and the thickness of the PZT patch respectively and K_s the structure's static stiffness.

* Corresponding author. Tel.: +91 11 2659 1040; fax: +91 11 2658 1117.
E-mail addresses: sumedha_maharana@yahoo.in (S. Moharana), sbhalla@civil.iitd.ac.in (S. Bhalla).

0020-7683/$ - see front matter © 2013 Elsevier Ltd. All rights reserved.
http://dx.doi.org/10.1016/j.ijsolstr.2013.12.022

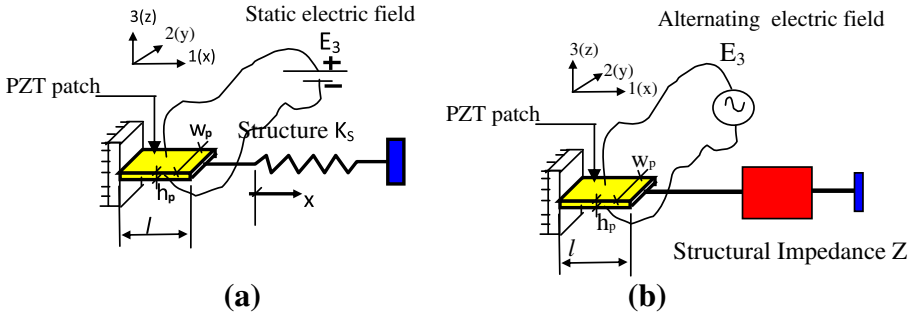

Fig. 1. Modeling of PZT-structure interaction (a) Static approach. (b) Impedance approach.

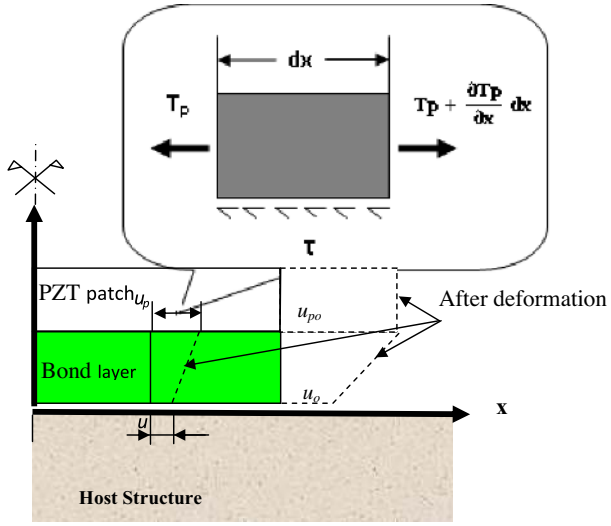

Fig. 2. Force/strain transfer mechanism through adhesive bond layer.

The main drawback of the static approach was that the inertia and the damping effects due to the bond layer were completely ignored.

In order to eliminate the limitations of the static approach, Liang and co-workers (1994) proposed the impedance based modelling approach. The related model is shown in Fig. 1(b). They started from the following governing equilibrium equation

$$\overline{Y^E}\frac{\partial^2 u_p}{\partial x^2} = \rho\frac{\partial^2 u_p}{\partial t^2} \tag{4}$$

where u_p is the displacement of the PZT patch and ρ its density. Here, dynamic equilibrium is considered and complex Young's modulus of elasticity has been used. Solving Eq. (4) and integrating the resulting strain into piezo-converse relation (Eq. (2)), the final expression for admittance can be derived as

$$\begin{aligned}\bar{Y} &= G + Bj \\ &= 2\omega j\frac{w_p l}{h_p}\left[\left(\overline{\varepsilon_{33}^T} - d_{31}^2\overline{Y^E}\right) + \left(\frac{Z_a}{Z+Z_a}\right)d_{31}^2\overline{Y^E}\left(\frac{\tan kl}{kl}\right)\right]\end{aligned} \tag{5}$$

where Z_a is the actuator impedance, defined as

$$Z_a = \frac{kh_p w_p \overline{Y^E}}{j\omega\tan(kl)} \tag{6}$$

and k is wave number, which for 1D (one dimensional) case is given by

$$k = \omega\sqrt{\frac{\rho}{\overline{Y^E}}} \tag{7}$$

Although inertia effects are considered properly in the impedance approach, the effect of the adhesive layer has been ignored and the PZT patch is assumed to be connected to the structure at its ends only. Zhou et al. (1996) extended the 1D formulation of Liang to 2D piezo-bonded structure, but again ignoring the shear lag effects. Bhalla and Soh (2004a, b) introduced the definition of effective impedance by considering the force transfer to be distributed along the entire boundary of the PZT patch. By solving the governing 2D coupled wave equation, they derived a compact expression (as an alternative to complicated expression derived by Zhou et al., 1996) for coupled admittance signature as

$$\bar{Y} = G + Bj = 4\omega j\frac{l^2}{h_p}\left[\overline{\varepsilon_{33}^T} - \frac{2d_{31}^2\overline{Y^E}}{(1-\upsilon)} + \frac{2d_{31}^2\overline{Y^E}}{(1-\upsilon)}\left(\frac{Z_{a,eff}}{Z_{s,eff}+Z_{a,eff}}\right)\overline{T}\right] \tag{8}$$

where $Z_{s,eff}$ and $Z_{a,eff}$ are respectively the effective impedances of the structure and the PZT patch. Further, complex tangent ratio $\overline{T}$ was introduced with correction factors C_1 and C_2 for more accurate results (based on the experimental signature of freely suspended PZT patch) as

$$\overline{T} = \frac{1}{2}\left(\frac{\tan(C_1 kl)}{(kl)} + \frac{\tan(C_2 kl)}{(kl)}\right) \tag{9}$$

Again, the shear lag effect of the adhesive bond layer was ignored in this model.

Previously, it was assumed that the bond itself is very thin and is of negligible mass. But the presence of material discontinuity between the PZT patch and the host structure, in the form of adhesive bond layer, does influence the performance of the sensor due to shear lag effect. Crawley and de Luis (1987) were the first to consider the presence of the bond layer in force transmission mechanism involving PZT patches. They introduced the shear lag

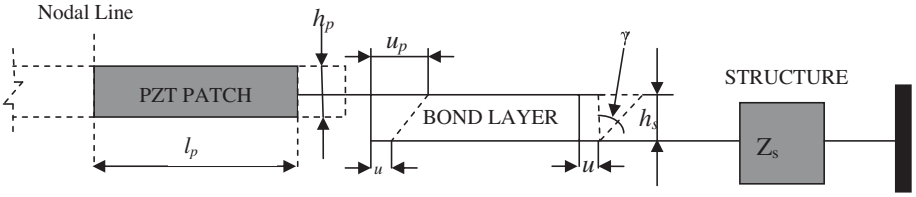

Fig. 3. Simplified 1D impedance model (Bhalla et al. 2009).

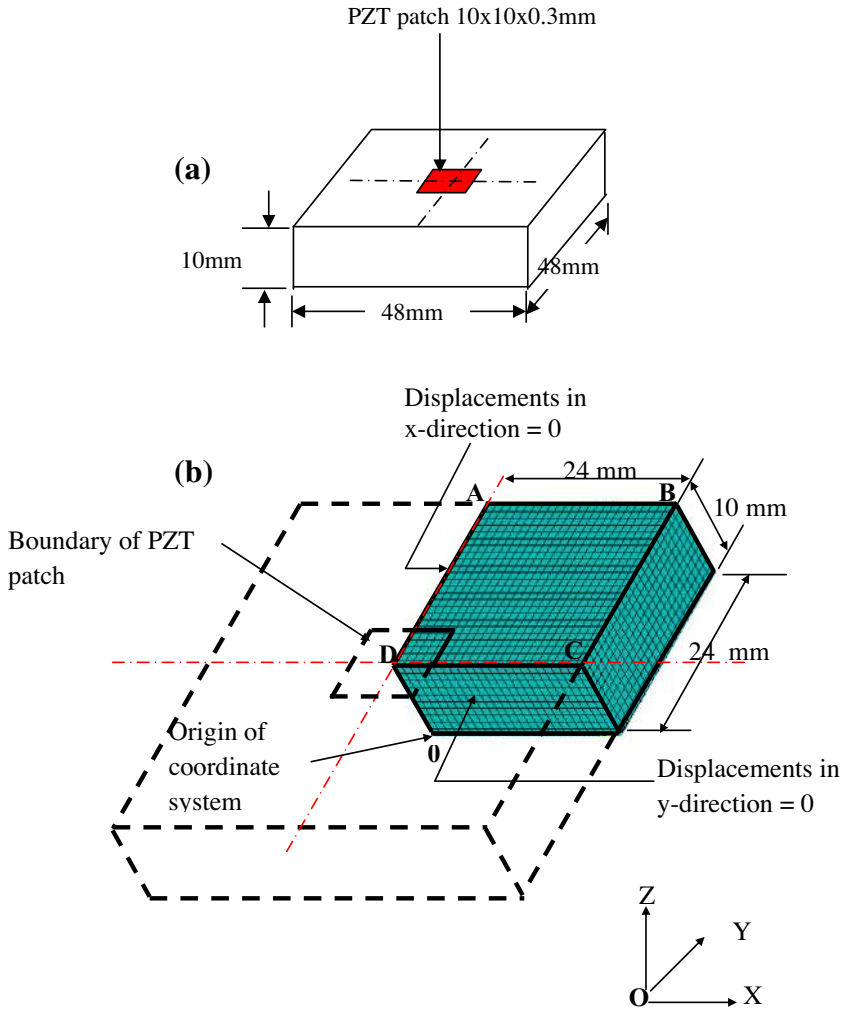

Fig. 4. (a) Aluminum block structure (b) Finite element model of a quarter of structure.

parameter, Γ, for the case of a PZT patch bonded to a beam structure, mathematically expressed as

$$\Gamma = \sqrt{\frac{G_s}{h_p h_s Y^E} + \frac{3G_s w_p}{Y_b w_b h_p h_s}} \tag{10}$$

where G_s is the shear modulus of the adhesive, Y_b the Young's modulus of elasticity of the beam, h_s the thickness of the adhesive layer and w_b the width of the beam. Sirohi and Chopra (2000) concluded through their analysis that for $\Gamma > 30\ \text{cm}^{-1}$, the strain is more or less effectively transferred to the ends of the PZT patch, for which case the bonding between the structure and the patch can be assumed to be perfect and shear lag effect can be neglected. However, their treatment was separate for sensing and actuation applications, and not suitable for the EMI technique, where the patch serves both the roles simultaneously.

Xu and Liu (2002) modelled the bond layer in the impedance approach as a single degree freedom (SDOF) system and derived a shear lag ratio (ξ) in terms of the dynamic stiffness of the bond layer (k_b) to that of structure (k_s), as

$$Z_{eq} = \left(\frac{k_b}{k_b + k_s}\right) Z_s = \xi Z_s \tag{11}$$

where "ξ" is the impedance modification parameter. Xu and Liu (2002), however, did not provide any explicit quantification of their parameter. Ong et al. (2002) partly integrated the shear transfer phenomena in the EMI technique by considering the effective length approach of Sirohi and Chopra (2000), based on the shear lag effect for sensing case only.

Bhalla and Soh (2004c) rigorously considered the shear lag effect by including the shear stress term in dynamic equilibrium equation (illustrated in Fig. 2) as

$$\tau w_p dx = \frac{\partial T_p}{\partial x} h_p w_p dx \tag{12}$$

where u_p is the displacement in the PZT patch, w_p the width of the PZT patch, τ the interfacial shear stress and T_p the stress in the

Table 1
Parameters of PZT patch, aluminum block and adhesive bond.

Material	Physical parameter	Value
PZT Patch	Electric permittivity ε_{33}^T (F/m)	1.7785×10^{-8}
	Peak correction factor (C_1,C_2)	0.898
	$k = \frac{2d_{31}^2 Y^E}{(1-\upsilon)}$ (N/V^2)	5.35×10^{-9}
	Mechanical loss factor η	0.0325
	Dielectric loss factor δ	0.0224
Aluminum Block	Young's modulus (GPa)	68.95
	Density (Kgm^{-3})	2715
	Poisson's ratio	0.33
	Rayleigh damping coefficients	
	α	0
	β	3×10^{-9}
Adhesive	Shear modulus (G_s) (GPa)	1
	Mechanical loss factor η'	0.1

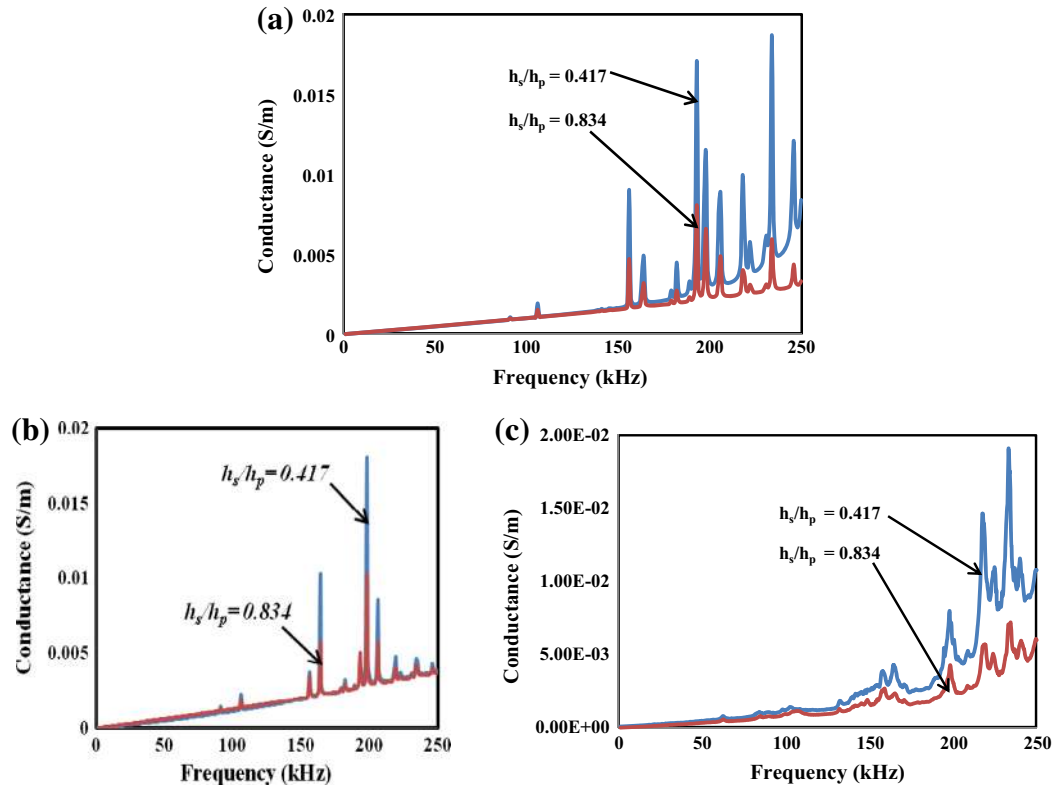

Fig. 5. Comparison of conductance of experimental result with continuum shear lag model. (a) Normalized analytical conductance (continuum model) for h_s/h_p = 0.417 and h_s/h_p = 0.834. (b) Normalized analytical conductance (Refined model) for hs/hp=0.417 and hs/hp=0.834. (c) Normalized experimental conductance for h_s/h_p = 0.417 and h_s/h_p = 0.834.

patch. The inertial term was, however, neglected in the derivation. For 1D case, they modified Eq. (8) by substituting (Z_s) by the equivalent structural impedance ($Z_{s,eq}$), that is

$$Z_{eq} = Z_s \frac{u_{(x=l)}}{u_{p(x=l)}} = \frac{Z_s}{\left(1 + \frac{u_0'}{u_0 \bar{p}}\right)} \tag{13}$$

where u_0 and u_0' are the displacement and the strain respectively at the interface between the adhesive layer and the host structure at $x = l$ (see Fig. 2). The shear lag parameter $\bar{p}$ was defined as

$$\bar{p} = -\frac{w_p \overline{G_s}}{Z_s h_s j\omega} \tag{14}$$

where $\overline{G_s} = G_s(1 + \eta' j)$ is the complex shear modulus (η' being the mechanical loss factor of adhesive bond). The model was extended to 2D case also. Later, another simplified model was proposed by Bhalla et al. (2009), where the bond layer was modelled as a connecting shear element (attached between the PZT patch and the structure) and assuming the entire system to be under pure shear mechanism, as shown in Fig. 3. For this case, Bhalla et al. (2009) expressed the equivalent structural impedance in much simpler term compared to the previous model, as

$$Z_{s,eq} = \frac{Z_s}{\left[1 - \left(\frac{Z_s \omega h_s j}{w_p \overline{G_s}}\right)\right]} \tag{15}$$

Although the above models attempted to include shear transfer mechanism in EMI technique with relation of force- impedance mechanism, they ignored the effect of inertial mass term for simplicity, which otherwise plays a significant role in bringing down the peaks of the admittance signatures. In addition, the admittance signature ($\overline{Y}$) derived by the above approaches has shortcoming that the equivalent structural impedance ($Z_{s,eq}$), is computed at ($x = l$) only (see Eq. (13)). Improvement on this front was done by Bhalla and Moharana (2013), which is briefly described in next section. Several other researchers have also analyzed the effects of the adhesive layer between the surface bonded PZT patch and the host structure for structural monitoring and control (Pietrzakowski, 2001; Han et al., 2008; Dugnani, 2009; Ha and Chang, 2010; Huang et al., 2010; Dugnani, 2013).

2. Refined shear lag model

Bhalla and Moharana (2013) proposed a refined shear lag model duly considering the inertia term together with the shear term in Eq. (12), that is

$$\tau w_p dx + (dm)\frac{\partial^2 u_p}{\partial t^2} = \frac{\partial T_p}{\partial x} h_p w_p dx \tag{16}$$

They simplified the equation as

$$\bar{\alpha} u_p - u = \frac{1}{q} u_p'' \tag{17}$$

where a new factor $\bar{\alpha} = 1 - \frac{\rho h_p h_s \omega^2}{\overline{G_s}}$ was introduced to take care of the inertia effects. q is the previously defined second shear lag parameter, given by (Bhalla and Soh, 2004c)

$$q = \frac{\overline{G_s}}{\overline{Y^E} h_s h_p} \approx \frac{G_s}{Y^E h_p h_s} \tag{18}$$

The remarkable improvement over previous model (Bhalla and Soh, 2004c) is the inclusion of factor $\bar{\alpha}$, which was taken as unity in the previous models. Further, the second necessary equation was derived more accurately based on shear force transfer mechanism along the adhesive bond length, that is

$$\int_x^l \frac{w\overline{G_s}(u_p - u)dx}{h_s} = Z_s j\omega u \tag{19}$$

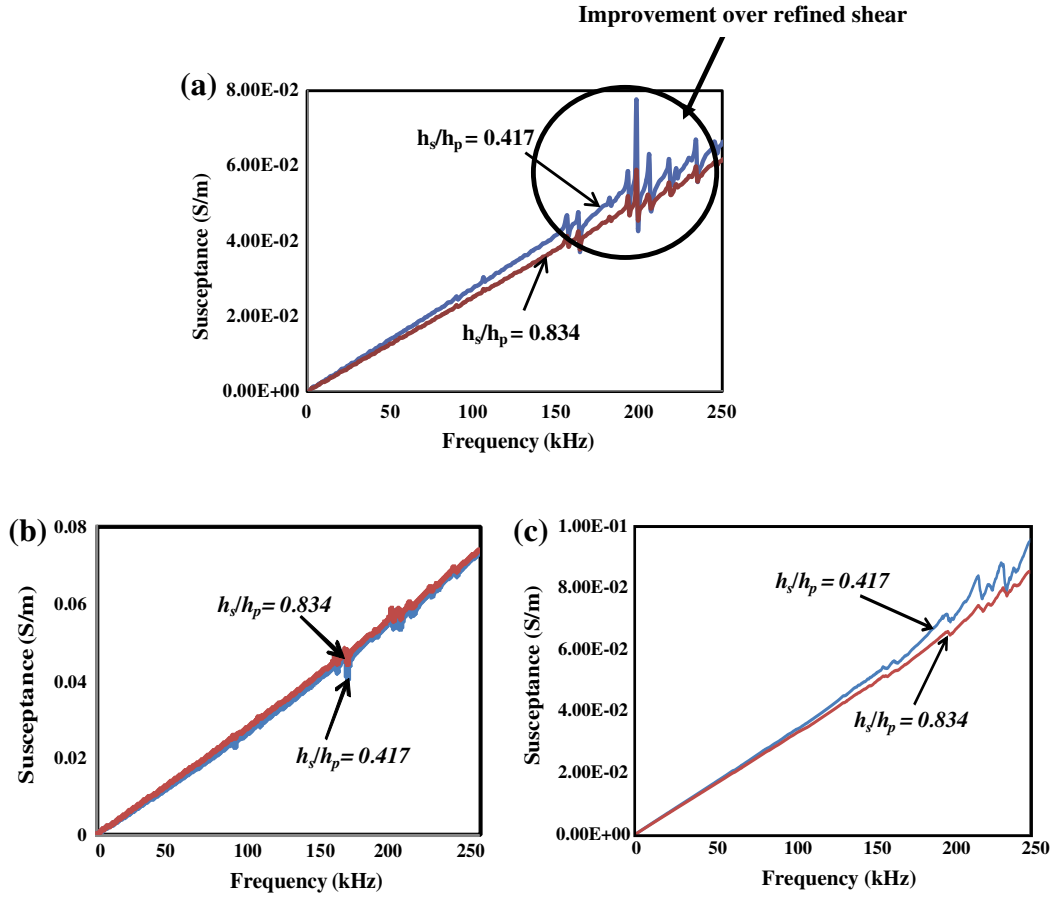

Fig. 6. Comparison of susceptance of experimental result with continuum shear lag model. (a) Normalized analytical susceptance (continuum model) for $h_s/h_p = 0.417$ and $h_s/h_p = 0.834$. (b) Normalized analytical susceptance (Refined model) for hs/hp=0.417 and hs/hp=0.834. (c) Normalized experimental susceptance for $h_s/h_p = 0.417$ and $h_s/h_p = 0.834$.

Differentiating both sides with respect to x and simplifying, we get

$$u_p = u + \frac{u'}{\bar{p}} \tag{20}$$

Substituting Eq. (20) in Eq. (17) and simplifying, the refined governing differential equation was derived as

$$u''' + \bar{p}u'' - \bar{\alpha}qu' + (1-\bar{\alpha})\bar{p}qu = 0 \tag{21}$$

The solution for u and u_p was obtained by imposing appropriate boundary conditions after which the equivalent mechanical impedance was obtained using Eq. (13). Similar procedure was followed for 2D refined shear lag case. The signatures resulting from the refined model exhibited a better match with the experimental signatures. The main shortcoming here, however is that the values are determined by making approximate computation from the true structural impedance (Eq. (13)). However, in order to rigorously consider the shear transfer phenomena through the adhesive layer, one needs to integrate all terms accounting for shear lag effect (all adhesive properties) and the forces encountered in the strain equilibrium equation continuously and simultaneously, which has not been attempted so far for the EMI technique. This is the main objective addressed in the paper, discussed in the forthcoming sections.

In practical applications, where the strains are a source for control, the term "actuation strain" refers to the strain other than that caused by external stresses (generated due to application of external force and boundary conditions), such as thermal, magnetic or piezoelectric effects. Thus, the actuation strain is the term $\Lambda = d_{31}E_3$. For an unconstrained, unstressed piezoelectric material, the induced strain would be the same as actuation strain. However, if the piezoelectric patch is constrained, being embedded or bonded with another material, the actuation strain is clearly different from the induced strain. The induced strain is influenced by the actuation strain and it is determined by the coupling term at electro-mechanical interaction. Hence, an accurate calculation of the actuation strain duly considering the adhesive effect along and throughout the total bond area will achieve the more accurate coupled admittance signature. In this paper, this is improved using continuum based approach, as will be covered in following sections.

3. Derivation of admittance signature using continuum approach

The electric displacement D_3 over the surface of a PZT patch can be determined from the basic equations governing piezoelectric direct effect. For 2D case, the piezoelectric constitutive equations can be reduced to (Bhalla and Soh, 2004a)

$$D_3 = \overline{\varepsilon_{33}^T}E_3 + d_{31}(T_1 + T_2) \tag{22}$$

$$S_1 = \left(\frac{T_1 - \upsilon T_2}{\overline{Y^E}}\right) + d_{31}E_3 \tag{23}$$

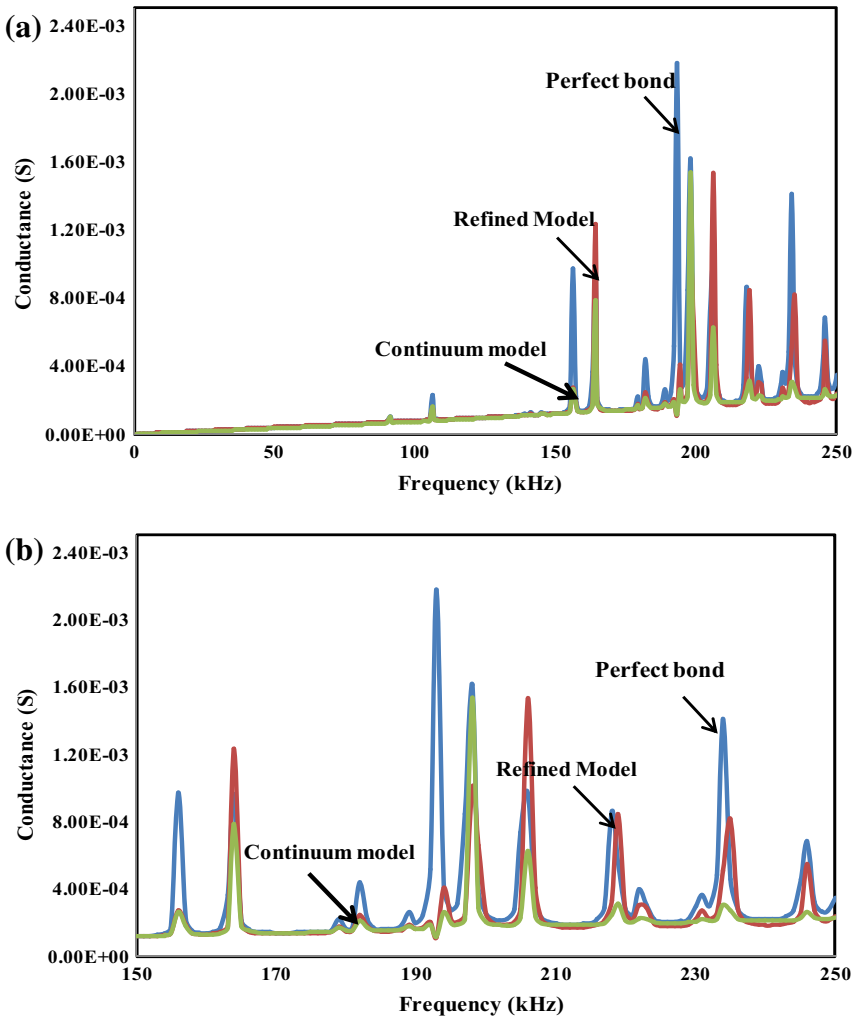

Fig. 7. Comparison of conductance (G) plot. (a) Plot over (0–250) kHz. (b) Closer view (150–250) kHz.

$$S_2 = \left(\frac{T_2 - \upsilon T_1}{\overline{Y^E}}\right) + d_{31}E_3 \tag{24}$$

where υ is the Poisson's ratio of the patch and T_1, T_2 and S_1, S_2 are the principal components of stress and strain tensor respectively. From Eqs. (23) and (24), we get

$$T_1 + T_2 = \frac{\overline{Y^E}}{(1-\upsilon)}(S_1 + S_2 - 2d_{31}E_3) \tag{25}$$

Substituting Eq. (25) into (22) and with $E_3 = \left(\frac{V_0}{h}\right)e^{j\omega t}$ (where V_0 represents the peak sinusoidal voltage), the equation can be further reduced to

$$D_3 = \overline{\varepsilon_{33}^T}\frac{V_0}{h}e^{j\omega t} + d_{31}\frac{\overline{Y^E}}{(1-\upsilon)}\left(S_1 + S_2 - 2d_{31}\frac{V_0}{h}e^{j\omega t}\right) \tag{26}$$

The current flowing through the circuit can be determined as

$$\bar{I} = \iint_A \dot{D}_3 dxdy = j\omega \int\int_A D_3 dxdy \tag{27}$$

Substituting Eq. (26) into Eq. (27), the equation can be written as (integrating from $x = 0$ to $x = l$ and multiplying a factor of 4).

$$\bar{I} = j\omega \iint_A \overline{\varepsilon_{33}^T}\frac{V_0}{h}e^{j\omega t}dxdy + j\omega \iint_A d_{31} \times \frac{\overline{Y^E}}{(1-\upsilon)}\left(S_1 + S_2 - 2d_{31}\frac{V_0}{h}e^{j\omega t}\right)dxdy \tag{28}$$

Substituting $\overline{V} = V_0 e^{j\omega t}$ ($\overline{V}$ represents the instantaneous voltage across the PZT patch), and solving the equation, it can be reduced to

$$\bar{I} = 4j\omega\overline{V}\frac{l^2}{h}\left[\overline{\varepsilon_{33}^T} - \frac{2d_{31}^2\overline{Y^E}}{(1-\upsilon)}\right] + j\omega d_{31}\frac{\overline{Y^E}}{(1-\upsilon)}\iint_A (S_1 + S_2)dxdy \tag{29}$$

The strains S_1 and S_2 can be obtained from the expressions for displacements (Bhalla and Moharana, 2013) as

$$\begin{aligned} S_1 &= -u'_{px} \\ &= \left(1 + \frac{\lambda_1}{\bar{p}_{eff}}\right)\lambda_1 e^{\lambda_1 x}A_1 + \left(1 + \frac{\lambda_2}{\bar{p}_{eff}}\right)\lambda_2 e^{\lambda_2 x}A_2 \\ &\quad + \left(1 + \frac{\lambda_3}{\bar{p}_{eff}}\right)\lambda_3 e^{\lambda_3 x}A_3 \end{aligned} \tag{30}$$

$$\begin{aligned} S_2 &= -u'_{py} \\ &= \left(1 + \frac{\lambda_1}{\bar{p}_{eff}}\right)\lambda_1 e^{\lambda_1 y}A_1 + \left(1 + \frac{\lambda_2}{\bar{p}_{eff}}\right)\lambda_2 e^{\lambda_2 y}A_2 \\ &\quad + \left(1 + \frac{\lambda_3}{\bar{p}_{eff}}\right)\lambda_3 e^{\lambda_3 y}A_3 \end{aligned} \tag{31}$$

The negative sign indicates that compressive strain is induced in the PZT patch on account of positive displacement at the patch tip. λ_1, λ_2 and λ_3 are the three complex roots of the shear lag

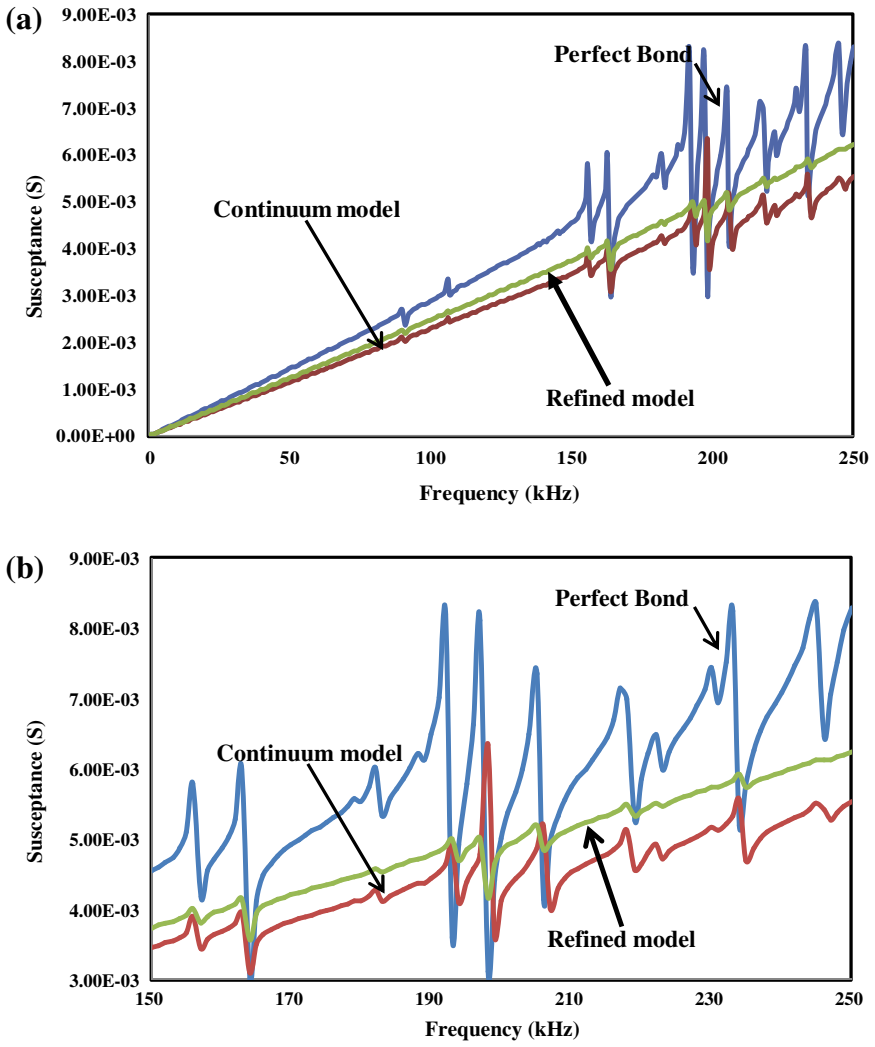

Fig. 8. Comparison of susceptance (B) plot. (a) Plot over (0–250) kHz. (b) Closer view (150–250) kHz.

governing differential equation of refined model (Bhalla and Moharana, 2013) and A_1, A_2 and A_3 are the three unknown coefficients of the solution, expressed as

$$u = A_1 e^{\lambda_1 x} + A_2 e^{\lambda_2 x} + A_3 e^{\lambda_3 x} \tag{32}$$

$\overline{p_{eff}}$, the shear lag parameter, suitable for the 2D case considered here, can be expressed as (Bhalla and Soh, 2004c)

$$\overline{p_{eff}} = -\frac{2l\overline{G_s}(1+\upsilon)}{Z_{eff} j\omega h_s} \tag{33}$$

The coefficients A_1, A_2 and A_3 can be determined from the imposed boundary conditions for refined model (Bhalla and Soh, 2004c). Using the expressions of S_1 and S_2 from Eqs. (30) and (31), the final complex electro-mechanical admittance spectra for full PZT patch can be obtained as

$$\overline{Y} = \frac{\bar{I}}{\bar{V}} \tag{34}$$

which, after simplifying , yields the final expression for $\bar{Y}$ as

$$\overline{Y} = 4j\omega\frac{l^2}{h_p}\left[\overline{\varepsilon_{33}^T} - \frac{2d_{31}^2\overline{Y^E}}{(1-\upsilon)}\right] - \frac{8lj\omega d_{31}\overline{Y^E}}{(1-\upsilon)\bar{V}}\left[\left(1+\frac{\lambda_1}{\bar{p}_{eff}}\right)\lambda_1(e^{\lambda_1 l}-1)A_1 + \left(1+\frac{\lambda_2}{\bar{p}_{eff}}\right)\lambda_2(e^{\lambda_2 l}-1)A_2 + \left(1+\frac{\lambda_3}{\bar{p}_{eff}}\right)\lambda_3(e^{\lambda_3 l}-1)A_3\right] \tag{35}$$

In compact form, the coupled complex admittance can thus be expressed as

$$\overline{Y} = \frac{\bar{I}}{\bar{V}} = 4j\omega\frac{l^2}{h_p}\left[\overline{\varepsilon_{33}^T} - \frac{2d_{31}^2\overline{Y^E}}{(1-\upsilon)}\right] - \frac{8lj\omega d_{31}\overline{Y^E}}{(1-\upsilon)\bar{V}}[U_{con}] \tag{36}$$

where U_{con} is the continuum displacement generated at the interfacial bond layer after accounting the shear lag effect in the continuous manner as derived above. The main advantage of the new formulation is that it eliminates the equivalent structural impedance terms inherent in the previous models, which were based simply on approximation (see Eq. (13)). In the present approach, the admittance $\bar{Y}$ is determined by continuous integration, duly taking account of variation of stresses and strains along the PZT patch, rather than at the periphery of the patch. Since u and u_p were just considered at ends of the patch in previous models, they do not carry complete information behind the force transfer mechanism occurring along the adhesive bond. On the other hand, the term U_{con} takes care of the strain generated at interfacial bond due to PZT patch deformation in a continuous manner. This makes the current shear lag model more accurate and realistic.

4. Experimental comparisons

The admittance signature ($\overline{Y}$) derived in the previous section is verified in this section based on the experimental results of

Bhalla and Soh (2004a, b). The experimental set up consisted of an aluminium block (grade Al 6061-T6), $48 \times 48 \times 10$ mm in size, instrumented with a PZT patch of size $10 \times 10 \times 0.3$ mm (grade PIC 151, PI Ceramic 2003), as shown in Fig. 4(a). A bond thickness ($h_s = 0.125$ mm) was chosen for analytical and experimental signatures. This thickness was achieved in the test specimens by placing two parallel optical fibres on the surface of the host structure before bonding the PZT patch. Table 1 lists the key physical parameters of the PZT patch, the aluminium block and the adhesive. Fig. 4(b) shows the 3D finite element model of a quarter of the test structure, modelled to determine the numerical structural impedance (Z_s) by applying unit distributed force at particular frequency After performing harmonic analysis. The final admittance signature was determined using Eq. (36).

Figs. 5 and 6 compare the continuum, refined and experimental conductance and susceptance signatures respectively for two different bond thickness ratio ($h_s/h_p = 0.417$) and ($h_s/h_p = 0.834$). Figs. 7 and 8 respectively compare the conductance and susceptance signatures resulting from the continuum approach with those from the refined model and perfect bond. It can be clearly observed that the continuum signatures match closer to the experimental plots as compared to refined model (see Figs. 5(a), (b), and 6(a), (b)). For the susceptance, the influence of bond is significantly observed as the lowering the slope (see Figs. 6 and 8), which is not observed in the refined model. Similar observations hold good for conductance (Figs. 5 and 7). The accuracy and reliability of bonding effect on piezo-structure elastodynamic interaction has been increased significantly through continuum based approach, due to more effective quantification of the shear parameter throughout the bond area, which was lacking in the previous models.

5. Parametric study based on continuum model

Fig. 9 shows the effect of the mechanical loss factor η with two extreme variations (80% and 150%) on conductance and susceptance signatures based on the analysis carried out using the continuum model. The effect of damping of the bond layer has very negligible effect on overall signature, as clearly apparent from the figure. Fig. 10 shows the influence of the shear modulus of the bond layer on the signature. The effect is similar to that observed for the refined model (Bhalla and Moharana, 2013). Similarly, the effect of the dielectric loss factor δ on the admittance

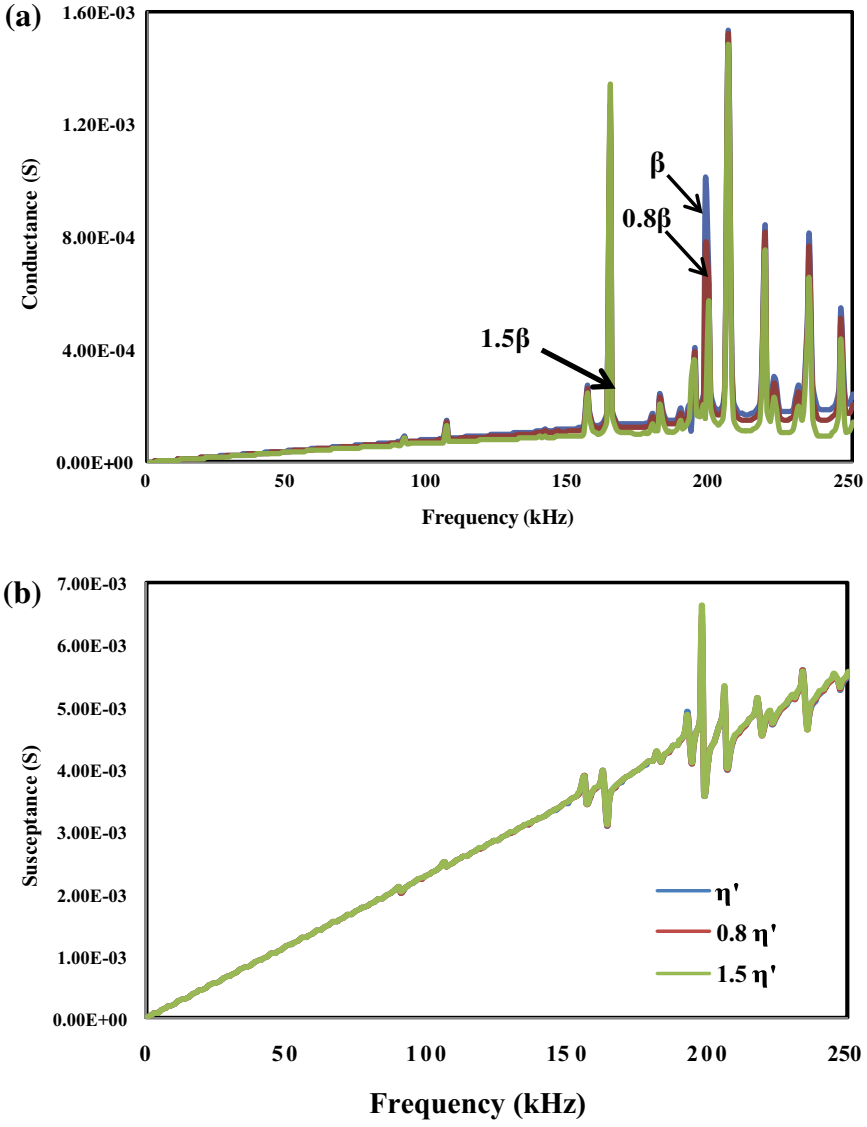

Fig. 9. Effect of mechanical loss of bond layer on new proposed admittance function. (a) Conductance vs Frequency. (b) Susceptance vs frequency.

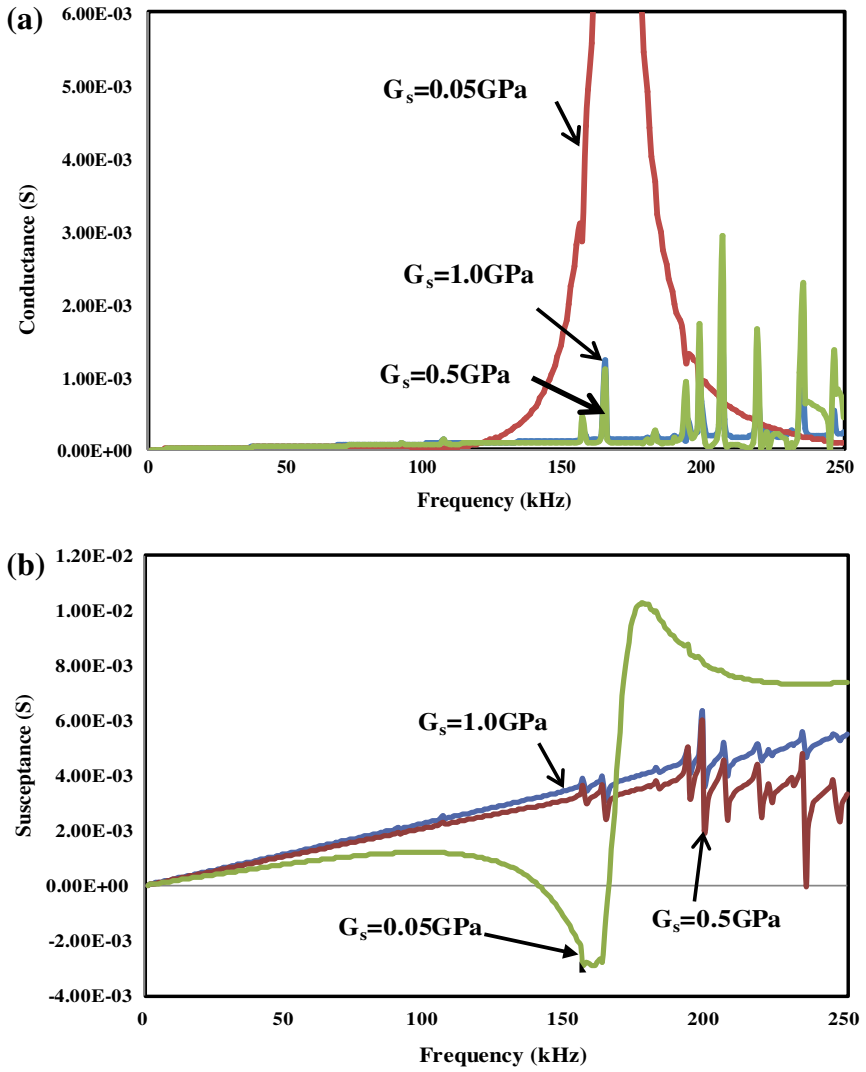

Fig. 10. Effect of shear modulus of bond layer on new proposed admittance function. (a) Conductance vs frequency. (b) Susceptance vs frequency.

signature is shown in Fig. 11 for a wide range of variation (80% and 150%), from which it is apparent that the effect of the dielectric loss is significant for conductance but negligible for susceptance. It can also be noted that compared to η, δ has much more significant effect on the conductance signature. The dimensional ratio (l^2/h) also has observable effect on normalized conductance (Gh/l^2) and normalized susceptance (Bh/l^2), as evident from Fig. 12. Hence, the PZT patch's dimensions has significantly affect the resulting admittance values. Form this study, it can be concluded that for better electro-mechanical interaction, sensor length and bond thickness should be minimum and $\overline{G_s}$ should be maximized.

6. Effect of adhesive mass on continuum based admittance signature

The combined effect of the inertia of both the adhesive and the PZT patch on the continuum based EMI admittance spectra is investigated in this section. The inertia term in the dynamic equilibrium equation (Eq. (16)) is replaced by

$$(dm_p)\ddot{u}_p + (dm_s)\ddot{u}_s \tag{37}$$

where dm_p and dm_s are the differential masses of the PZT patch and the adhesive respectively and $\ddot{u}_p$ and $\ddot{u}_s$ respectively denote the corresponding velocities. The average velocity is considered for adhesive layer.

Substituting Eq. (37) into (16) and solving, we get

$$\overline{\alpha'}u_p - \overline{\beta}u = \frac{1}{\overline{q}}u_p'' \tag{38}$$

where ($\overline{\alpha'}$ and $\overline{\beta}$) are the two inertia parameters, given by

$$\overline{\alpha'} = 1 - \frac{\left(\rho h_p + \frac{\rho_s h_s}{2}\right)h_s\omega^2}{\overline{G_s}} \tag{39}$$

$$\text{and } \overline{\beta} = 1 + \frac{\rho_s h_s^2 \omega^2}{2\overline{G_s}} \tag{40}$$

where ρ and ρ_s are the densities of PZT patch and adhesive respectively. The relation between u and u_p can be deduced form the shear stress transfer mechanism, (Bhalla and Moharana, 2013) expressed as

$$u_{p,eff} = u_{eff} + \frac{u'_{eff}}{\overline{p}_{eff}} \tag{41}$$

Substituting Eq. (41) into (38) and solving, the new modified shear lag equation for combined inertia effect can be rewritten as

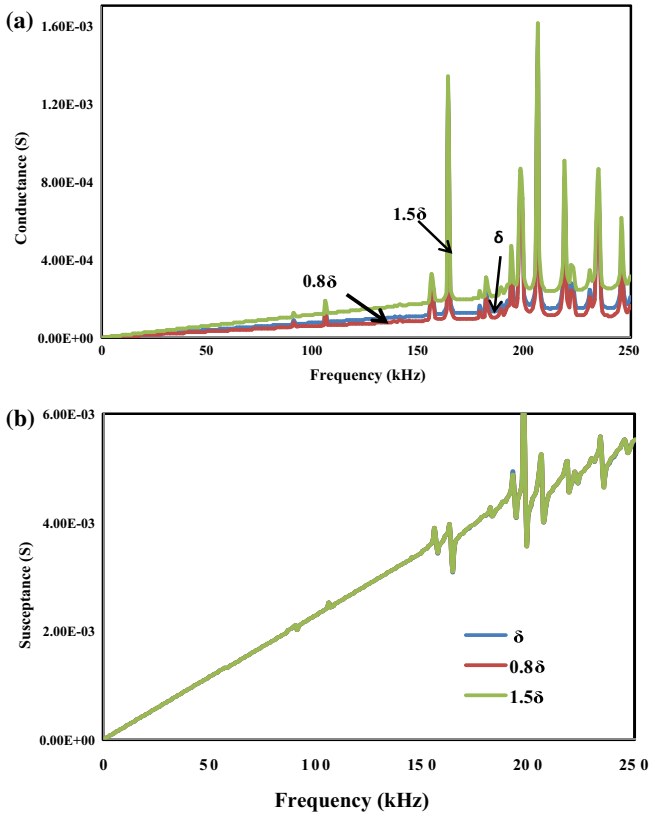

Fig. 11. Effect of dielectric loss on new proposed admittance function. (a) Conductance vs frequency. (b) Susceptance vs frequency.

$$u''''_{eff} + \bar{p}_{eff} u''_{eff} - \overline{\alpha'} q_{eff} u'_{eff} - (\overline{\alpha'} - \overline{\beta}) \bar{p}_{eff} q_{eff} = 0 \tag{42}$$

Eq. (42) was solved for both u and u_p (and hence strain S_p), which can be directly integrated into Eq. (30) followed by Eq. (36) to obtain more precise coupled admittance signature for the cumulative inertia effect of both the adhesive and PZT mass based on the continuum approach. Fig. 13 shows the overall effect on the admittance signature. The variation is not much significant for addition of inertia of adhesive on overall performance. Hence, the effect of inertia of adhesive layer can be neglected.

7. Conclusions

This paper has rederived the coupled admittance signature based on the continuous variation of displacement (hence, the related piezo induced strain) and charges over the PZT patch. This is more accurate and realistic shear lag model for the impedance based SHM for the EMI technique. A new continuum strain term (U_{con}) has been introduced to consider the continuous interaction of the bonding effect throughout the bond layer. It is more convenient and practical in real life applications because it eliminates all the approximations associated with previous models, which were based on equivalent impedance term without rigorous integration of all shear lag parameters (shear stress and inertia force) in a continuous manner. The continuum based signatures are qualitatively better match with experimental observations. The effect of the adhesive mass and the PZT mass simultaneously has also been investigated, which shows negligible impact on overall performance. Parametric study has been carried out to analyse the effect of both mechanical and electrical properties on the proposed

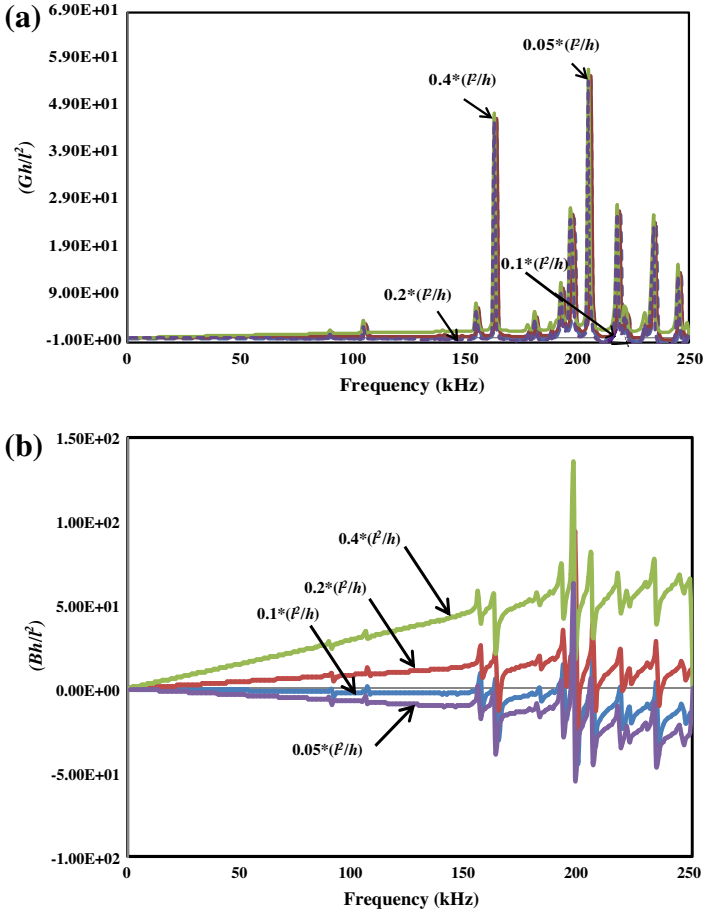

Fig. 12. Effect of dimension change (l^2/h) on new proposed admittance function. (a) Normalized conductance vs frequency. (b) Normalized susceptance vs frequency.

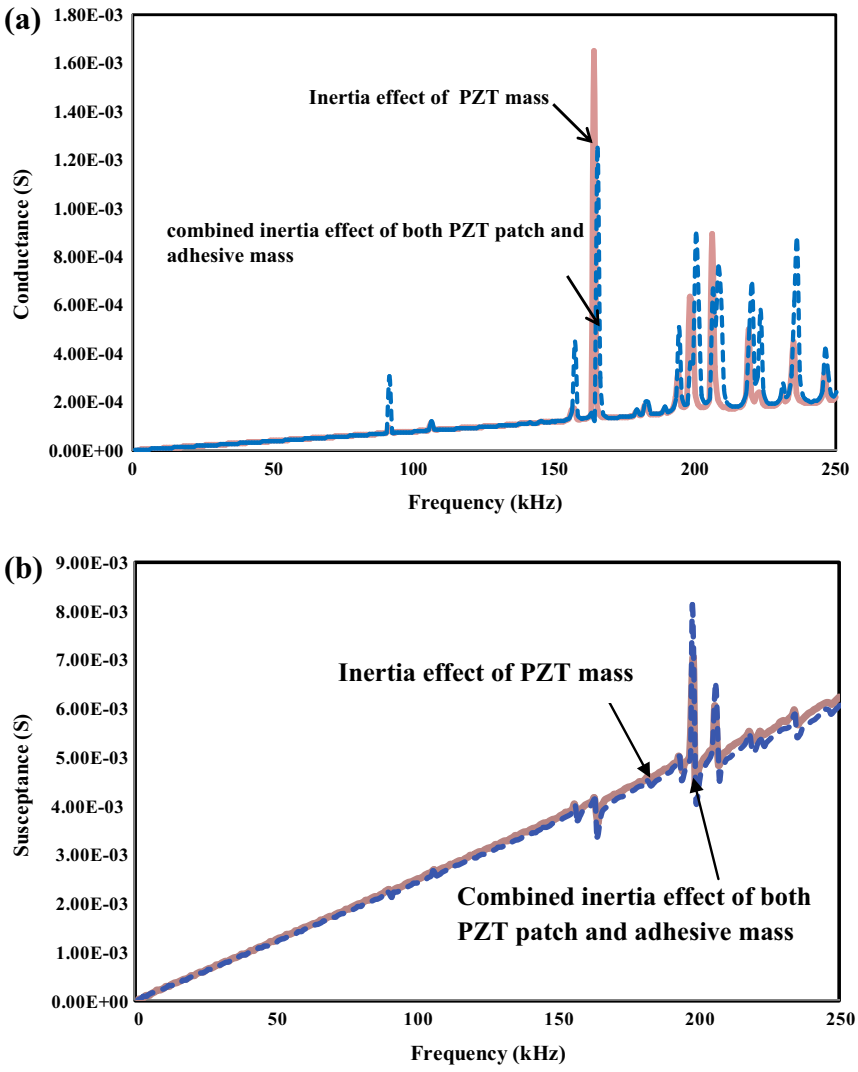

Fig. 13. Effect of combined mass (PZT and adhesive) effect on admittance signature. (a) Conductance vs. frequency. (b) Susceptance vs frequency.

admittance spectrum. The continuum model represents a significant improvement over the previous models.

References

Bhalla, S., Soh, C.K., 2003. Structural impedance based damage diagnosis by piezo-transducers. Earthquake Eng. Struct. Dyn. 32 (12), 1897–1916.

Bhalla, S., Soh, C.K., 2004a. Structural health monitoring by piezo-impedance transducers I: modelling. J. Aerosp. Eng. ASCE 17 (4), 154–165.

Bhalla, S., Soh, C.K., 2004b. Structural health monitoring by piezo-impedance transducers II: applications. J. Aerosp. Eng. ASCE 17 (4), 166–175.

Bhalla, S., Soh, C.K., 2004c. Impedance based modelling for adhesively bonded piezo-transducers. J. Intell. Mater. Syst. Struct. 15 (12), 955–972.

Bhalla, S., Yang, Y.W., Zhao, J., Soh, C.K., 2005. Structural health monitoring of underground facilities- technological issues and challenges. Tunnelling Underground Space Technol. 20 (5), 487–500.

Bhalla, S., Kumar, P., Gupta, A., Datta, T.K., 2009. Simplified impedance model for adhesively bonded piezo–impedance transducers. J. Aerosp. Eng. ASCE 22 (4), 373–382.

Bhalla, S., Moharana, S., 2013. A refined shear lag model for adhesively bonded piezo-impedance structure. J. Intell. Mater. Syst. Struct. 24 (1), 33–48.

Crawley, E.F., de Luis, J., 1987. Use of piezoelectric actuators as elements of intelligent structures. AIAA J. 25 (10), 1373–1385.

Dugnani, R., 2009. Dynamic behaviour of structure-mounted disk-shape piezoelectric sensors including the adhesive layer. J. Intell. Mater. Syst. Struct. 20, 1553–1564.

Dugnani, R., 2013. Monitoring adhesive integrity of disk-shaped transducer by electromechanical impedance. J. Intell. Mater. Syst. Struct. 24 (15), 1912–1923.

Giurgiutiu, V., Zagrai, A.N., 2000. Characterization of piezoelectric wafer active sensors. J. Intell. Mater. Syst. Struct. 11 (12), 959–976.

Giurgiutiu, V., Zagrai, A.N., 2002. Embedded self-sensing piezoelectric active sensors for on-line structural identification. J. Vib. Acoust. ASME 124 (1), 116–125.

Ha, S., Chang, F.K., 2010. Adhesive interface layer effects in PZT-induced lamb wave propagation. Smart Mater. Struct. 19 (2), 1–9.

Han, L., Wang, X.D., Sun, Y., 2008. The effect of bonding layer properties on the dynamic behaviour of surface bonded piezoelectric sensors. Int. J. Solids Struct. 45, 5599–5612.

Huang, G., Song, F., Wang, X., 2010. Quantitative modeling of coupled piezo-elasto dynamic behavior of piezoelectric actuators bonded to an elastic medium for structural health monitoring: a review. Sensors 10, 3681–3702.

IEEE, 1987. IEEE Standard on Piezoelectricity, Std. 176, IEEE/ANSI.

Liang, C., Sun, F.P., Rogers, C.A., 1994. Coupled electro-mechanical analysis of adaptive material systems- determination of the actuator power consumption and system energy transfer. J. Intell. Mater. Syst. Struct. 5, 12–20.

Lim, Y.Y., Bhalla, S., Soh, C.K., 2006. Structural identification and damage diagnosis using self-sensing piezo-impedance transducers. Smart Mater. Struct. 15 (4), 987–995.

Ong, C.W., Yang, Y., Wong, Y.T., Bhalla, S., Lu, Y., Soh, C.K., 2002. The effects of adhesive on the electro-mechanical response of a piezoceramic transducer coupled smart system. In: Proc. ISSS-SPIE International Conference on Smart Materials, Structures and Systems, 12–14 December, Bangalore, pp. 191–197.

Park, G., Cudney, H.H., Inman, D.J., 2000a. Impedance-based health monitoring of civil structural components. J. Infrastruct. Syst. ASCE 6 (4), 153–160.

Park, G., Cudney, H.H., Inman, D.J., 2000b. An integrated health monitoring technique using structural impedance sensors. J. Intell. Mater. Syst. Struct. 11, 448–455.

PI Ceramic, 2003. Product catalogue, Lindenstrabe, Germany. http://www.piceramic.de.

Pietrzakowski, M., 2001. Active damping of beams by piezoelectric system: effect of bonding layer properties. Int. J. Solids Struct. 37, 7885–7895.

Sirohi, J., Chopra, I., 2000. Fundamental understanding of piezoelectric strain sensors. J. Intell. Mater. Syst. Struct. 11 (4), 246–257.

Shanker, R., Bhalla, S., Gupta, A., 2011. Dual use of PZT patches as sensors in global dynamic and local EMI techniques for structural health monitoring. J. Intell. Mater. Syst. Struct. 22 (16), 1841–1856.

Soh, C.K., Tseng, K.K.H., Bhalla, S., Gupta, A., 2000. Performance of smart piezoceramic patches in health monitoring of a RC bridge. Smart Mater. Struct. 9 (4), 533–542.

Sun, F.P., Chaudhry, Z., Rogers, C.A., Majmundar, M., Liang, C., 1995. Automated real–time structure health monitoring via signature pattern recognition. In: Proc., SPIE Conference on Smart Structures and Materials Conference, San Diego, California, Feb. 27–Mar1, 2443, pp. 236–247.

Xu, Y.G., Liu, G.R., 2002. A modified electro-mechanical impedance model of piezoelectric actuator-sensors for debonding detection of composite patches. J. Intell. Mater. Syst. Struct. 13 (6), 389–396.

Zhou, S.W., Liang, C., Rogers, C.A., 1996. An impedance-based system modelling approach for induced strain actuator-driven structures. J. Vib. Acoust. ASME 118 (3), 323–331.